Polymer Chemistry

ROYAL SOCIETY OF CHEMISTRY

PAPER

View Article Online
View Journal | View Issue

Cite this: *Polym. Chem.*, 2025, **16**, 2117

Microneedle-mediated transdermal H_2S gas therapy for psoriasis†

Yanlin Wang, ‡[a] Fan Rong, ‡[b] Xiaoyi Sun,‡[a] Duohang Bi,‡[a] Yin Wang, *[b] Yijing Liu *[a,c] and Jintao Zhu *[a]

Received 15th December 2024,
Accepted 1st April 2025

DOI: 10.1039/d4py01431f

rsc.li/polymers

Psoriasis is a common chronic skin disease. Current psoriasis treatments face challenges such as low drug bioavailability and side effects. Hydrogen sulfide (H_2S) can be a potential therapeutic for psoriasis, while developing an effective delivery system and a controlled release strategy is essential to guarantee its efficacy and safety. We report a responsive microneedle (MN)-mediated transdermal H_2S gas therapy for treating psoriasis. The phenylboronic acid-modified hyaluronic acid (HP) and a peptide H_2S donor (AlaCOS) are synthesized, which assemble into H_2S donating nanoparticles (HP-AC NPs). The HP-AC NPs efficiently release AlaCOS in aqueous solution or acidic conditions, which can further release H_2S triggered by aminopeptidase N (APN) and carbonic anhydrase (CA). Moreover, the HP-AC NPs can effectively downregulate the pro-inflammatory cytokines in macrophages. Furthermore, the HP-AC NP-loaded MNs (HP-AC MN) are prepared with sufficient mechanical strength to penetrate the stratum corneum barrier. In the psoriatic mouse model, the mice receiving the HP-AC MN treatment exhibit decreased epidermal thickness, reduced levels of pro-inflammatory cytokines, and induced M2 polarization of macrophages. This MN-mediated H_2S gas therapy represents a promising alternative for treating psoriasis.

1 Introduction

Psoriasis is a common chronic skin condition marked by red, scaly patches or plaques on the skin.[1–3] It significantly impacts both the physical and psychological well-being of patients. However, current therapeutic approaches face several challenges, including suboptimal drug utilization and the presence of adverse side effects.[2,4,5] As such, there is an urgent need to develop novel treatments that are both safe and efficacious for managing this condition.

Alternative therapies for psoriasis can be inspired by nature. Historically, hot springs have been recognized for their therapeutic properties, with sulfur-rich springs, in particular, demonstrating notable potential benefits for human health.[6] Research has shown that sulfur springs effectively decrease the production of pro-inflammatory cytokines while enhancing the synthesis of anti-inflammatory cytokines.[7] Moreover, immersion in sulfur-rich water has been demonstrated to significantly alleviate the symptoms of psoriasis.[8] Inspired by these findings, we propose that hydrogen sulfide (H_2S) may have therapeutic potential for treating psoriasis. Although H_2S gas has been studied for its benefits in wound healing,[9–11] anti-inflammatory responses,[12–14] and anticancer treatments,[15,16] its application in psoriasis therapy is largely unexplored. Therefore, further investigation into the feasibility of using H_2S gas for psoriasis treatment is needed.

To enhance the therapeutic efficacy of H_2S, two critical challenges must be addressed. First, the uncontrolled release of H_2S can undermine therapeutic outcomes. Second, efficient delivery methods targeting the skin are necessary to reduce potential side effects. Commonly used H_2S donors include sodium hydrosulfide (Na_2S) and GYY4137.[17–20] However, Na_2S is characterized by its instantaneous release of H_2S upon interaction with aqueous environments, which poses challenges for achieving controlled release. In contrast, GYY4137 requires strong acidic conditions to facilitate an adequate release of H_2S. As such, these donors fail to meet the requirements for controlled H_2S delivery. Developing H_2S donors capable of gen-

[a]*Hubei Key Laboratory of Bioinorganic Chemistry and Materia Medica, Hubei Engineering Research Center for Biomaterials and Medical Protective Materials, School of Chemistry and Chemical Engineering, Huazhong University of Science and Technology (HUST), Wuhan, 430074, China.*
E-mail: yijingliu@hust.edu.cn, jtzhu@mail.hust.edu.cn
[b]*Engineering Research Center of Cell & Therapeutic Antibody, Shanghai Frontiers Science Center of Drug Target Identification and Delivery, School of Pharmacy, Shanghai Jiao Tong University (SJTU), Shanghai, 200240, China.*
E-mail: yinwang@sjtu.edu.cn
[c]*Shenzhen Huazhong University of Science and Technology Research Institute, Shenzhen 518057, China*

†Electronic supplementary information (ESI) available. See DOI: https://doi.org/10.1039/d4py01431f

‡These authors contributed equally to this work.

erating H_2S in response to disease-specific microenvironments could solve this problem.

Traditional administration methods in psoriasis therapies include oral and topical routes. However, oral drugs are subject to the first-pass effect, limiting the amount of active drug reaching the lesion site.[21,22] Topical applications, on the other hand, are limited by low skin penetration efficiency due to the stratum corneum barrier.[23] Microneedles (MNs) present a minimally invasive and highly effective method for the transdermal delivery of therapeutic agents directly to psoriatic skin.[24–30] However, the feasibility of utilizing MN technology for H_2S gas therapy in treating psoriasis warrants further investigation.[31]

In this study, we report a responsive MN-mediated transdermal H_2S gas therapy for the treatment of psoriasis (Scheme 1). To achieve this, the phenylboronic acid-modified hyaluronic acid (HP) and a peptide H_2S donor (AlaCOS) were synthesized. Responsive H_2S donating nanoparticles (HP-AC NPs) were synthesized by combining HP and AlaCOS through the coordination of boron and nitrogen between the two components.[32,33] The HP-AC NPs efficiently release AlaCOS in aqueous solution or acidic conditions, which can further release H_2S triggered by aminopeptidase N (APN) and ubiquitous carbonic anhydrase (CA). Moreover, we showed that the HP-AC NPs could effectively downregulate the pro-inflammatory cytokines in macrophages. Furthermore, the HP-AC NP-loaded MNs were prepared with sufficient mechanical strength to penetrate the stratum corneum barrier. In the psoriatic mouse model, the mice receiving the HP-AC NP-loaded MN treatment exhibited decreased epidermal thickness, reduced levels of pro-inflammatory cytokines, and induced the M2 polarization of macrophages. This MN-mediated H_2S gas therapy represents a promising alternative for treating psoriasis and may also apply to other inflammatory skin diseases.

2 Experimental

2.1 Materials

Hyaluronic acid (HA, MW = 10 kDa) was purchased from Meilun Biotechnology Co., Ltd (China). 3-(Aminomethyl) phenylboronic acid hydrochloride (PBA) and 4-(4,6-dimethoxy [1.3.5] triazin-2-yl)-4-methylmorpholinium chloride (DMTMM) were purchased from Innochem Technology Co., Ltd (China). *N*,*N*′-Dimethylformamide (DMF, AR) was purchased from General Reagent Co., Ltd (China). Washington state probe-5 (WSP-5) was synthesized according to the reported method.[34] Cetyltrimethylammonium bromide (CTAB) was purchased from Aladdin Biochem Technology Co., Ltd (China). Enzyme-linked immunosorbent assay (ELISA) kits were purchased from Solarbio Life Science Co., Ltd (China). Sulfanilic acid (SA) and *N*-(1-naphthyl) ethylenediamine dihydrochloride (NED) were purchased from Titan Biotechnology Co., Ltd (China).

2.2 Synthesis and characterization of HP

HA (200 mg, 0.54 mmol) was added to a mixture of 6.6 mL of deionized water (DIW) and 3.4 mL of DMF. Once the HA was completely dissolved, PBA (75 mg, 0.40 mmol) and DMTMM (166 mg, 0.75 mmol) were added, and the pH of the solution was adjusted to 6.5. The mixture was then stirred at room temperature for 48 h. Afterward, the solution was transferred to a 3 kDa dialysis bag and dialyzed in DIW for 72 h, with the dialysis water being changed at regular intervals. The hydrophilic polymer (HP) can be obtained by freeze-drying the dialyzed solution. To characterize the successful grafting of PBA onto HA and to calculate the degree of substitution of PBA on HA, D_2O was used to dissolve the HP for proton nuclear magnetic resonance (^{1}H-NMR) analysis.

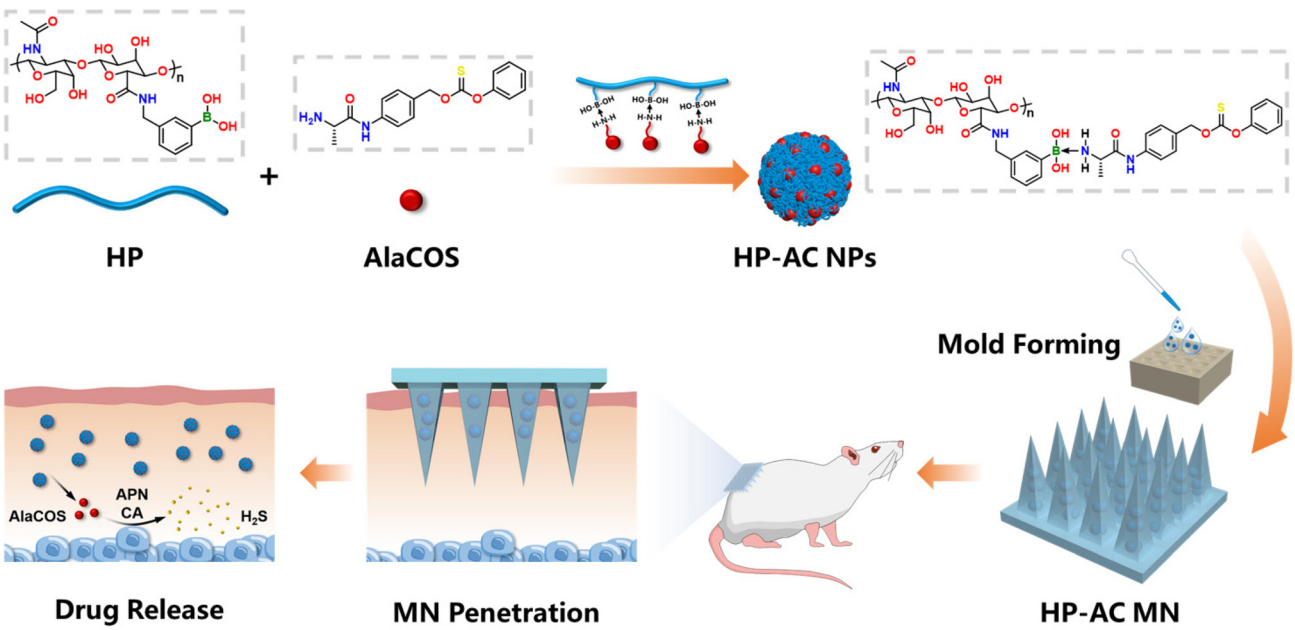

Scheme 1 Schematic illustration of the fabrication and application of H_2S donating HP-AC MN.

2.3 Synthesis and characterization of AlaCOS

AlaCOS was synthesized according to our previously reported route.[35] Mass spectrometry (MS), ^{1}H-NMR ^{13}C-NMR, and UV-Vis were employed to characterize the synthesized AlaCOS.

2.4 Preparation and characterization of HP-AC NPs

HP was dissolved in DIW to create a 25 mg mL^{-1} solution. It was then mixed with AlaCOS at a 10 : 1 mass ratio and subjected to vortex mixing and ultrasound treatment to obtain a uniform dispersion. After removing large aggregates by centrifugation, the HP-AC NPs (HP-AC NPs) were obtained.

To study the drug release, the absorption spectrum of AlaCOS in PBS solutions at concentrations of 2, 5, 10, 20, 40, and 60 μg mL^{-1} was measured using a UV-Vis spectrophotometer, and calibration curves were created accordingly. The solutions containing HP-AC NPs were placed in a 3 kDa dialysis bag and dialyzed against PBS solutions with pH values of 5.5 and 7.4 at 37 °C. Samples were collected at fixed time intervals (1, 2, 4, 8, 12, 24, 36, and 48 h), and the absorption spectra of the PBS solution were analyzed using a spectrophotometer. The amount of released drugs was calculated based on the standard curves obtained.

2.5 H_2S response released

H_2S releasing curves were measured using methylene blue assay. Briefly, each HP-AC NP dispersion was mixed with enzymes in 0.01 M PBS to make the final concentration of AlaCOS, APN, and CA 100 μM, 1 μg mL^{-1}, and 25 μg mL^{-1}, respectively. As a control, an equal volume of 0.01 M PBS solution without APN was added instead. The solutions were then incubated at 37 °C. At the set time points (10, 20, 30, 45, 60, 80, 120, 180 min), 100 μL of the solution was taken out and added to a well of the 96-well plate, followed by adding 25 μL of 20 mM *N*,*N*-dimethyl-1,4-phenylenediamine sulfate in 7.2 M HCl and 25 μL of 30 mM $FeCl_3$ in 1.2 M HCl. After storing in the dark for 60 min, the absorbance at 750 nm was measured using a microplate reader (Thermo Scientific Varioskan Flash). The concentration of H_2S was calculated using an H_2S calibration curve (using Na_2S as an H_2S source).

2.6 Cell experiment

Macrophages (designated as RAW264.7) were incubated with 1.5 mL of DMEM containing lipopolysaccharides (LPS) at a concentration of 100 ng mL^{-1} for 24 h to induce the M1 phenotype. Following this, the M1 macrophages were incubated with 1.5 mL of glucose-free DMEM containing either sodium sulfide (Na_2S) or HP-AC NPs at 37 °C. To measure the H_2S content in the cells, a mixture of WSP-5 (50 μM) and CTAB (200 μM) was added after a 6 h incubation, and the resulting green fluorescence signal was observed using a fluorescence microscope. For detecting nitric oxide (NO), the supernatant of the medium was mixed with sulfanilic acid (SA) and *N*-(1-naphthyl) ethylenediamine dihydrochloride (NED), and the absorbance was measured at 524 nm using a microplate reader. Additionally, an ELISA was performed on the supernatant to detect the TNF-α levels.

2.7 Fabrication and characterization of HP-AC MN patch

50 μL of the HP-AC NP dispersion was added onto a PDMS mold using a pipette. The solution was then gently smoothed out, and any bubbles present were removed. Following this, the mold was placed in an oven at 37 °C to evaporate most of the liquid. This process was repeated until the desired drug amount was loaded into the mold. For the final addition, 50 μL of a 100 mg mL^{-1} HA solution was added as the base, and the MN was returned to the oven until completely dried. Once dried, the MN was carefully removed from the mold.

Morphology of MN was characterized by a digital microscope and a scanning electron microscope. The confocal laser scanning microscope (CLSM) was used to characterize MN tips carrying fluorescein. The MN patch was inserted into a fresh pig skin sample and later removed, and the imaging of the skin at different depths after treatment was detected using CLSM.

The mechanical strength of MN patches was evaluated by testing the breaking point of MN patches with a universal texture tensile analyser.

2.8 Animal experiments

SPF BALB/c mice (16 females, 20–22 g) were purchased from Liaoning Changsheng Biotechnology Co., Ltd (Liaoning, China). All mice were kept at a constant temperature of 21 °C with an air humidity of 40%–70% and a 12 h/12 h light–dark cycle. All animal experiments were carried out under the guidance and approval of the Institutional Animal Protection and Use Committee of Tongji Medical College, Huazhong University of Science and Technology (Wuhan, China) (IACUC number: 4166). The mice were divided into four groups with four mice each: control, model, 1 MN, and 3 MN.

Before the study, hair was removed from the dorsal regions of all mice. 50 mg of imiquimod (IMQ) cream was applied to the backs of the mice in the model for five consecutive days to induce psoriasis-like mice. Starting from day 3rd, one MN patch (1 MN group) and three MN patches (3 MN group) were applied, respectively. The dorsal skin photographs and weights of mice were taken to assess the Psoriasis Area and Severity Index (PASI) score. On the day 6th, all mice were humanely sacrificed. Blood serum was extracted from the control group and the 3 MN group using centrifugation to assess liver and kidney function indexes. Subsequently, the heart, liver, spleen, lungs, and kidneys were harvested for hematoxylin–eosin (H&E) staining. Dorsal skin samples from all mice were collected for immunohistochemical analysis of the expression of Ki-67, CD206, CD86, TNF-α, IL-17, and IL-23. Additionally, the spleens of all mice were weighed, and the spleen index was calculated by comparing them to the body weight of each mouse.

3. Results and discussion

3.1 Synthesis of the H_2S donor and polymer carrier

First, the H_2S donor (AlaCOS) and polymer carriers of HP were synthesized. The presence of aminopeptidase N (APN) and carbonic anhydrase (CA) in the skin allows for the design of

enzyme-responsive H_2S donors for controlled release. APN is a membrane protein expressed on immune-related cells, such as macrophages and dendritic cells, which regulates the functions of inflammatory mediators.[36] CA can facilitate the dissociation of bicarbonate ions and their reverse reactions to adjust the acid–base balance in the tissue.[37] Elevated expressions of APN and CA have been observed in psoriatic skin, which may serve as potential internal stimuli for the controlled release of therapeutic agents.[38,39] Consequently, the enzyme-responsive H_2S donor was synthesized by sequentially conjugating Boc-alanine with 4-amino benzyl alcohol and phenyl chlorothionoformate, followed by deprotection (Fig. 1a). The successful synthesis of AlaCOS was confirmed by ^{1}H-NMR (Fig. 1c) and mass spectrum (Fig. S1†). To promote the stability and solubility of AlaCOS, the polymer carrier of HP was prepared by modifying HA with 3-aminophenyl boric acid (PBA), which can link with AlaCOS through the boron–nitrogen coordination[40–42] (Fig. 1b). ^{1}H-NMR spectrum of HP (Fig. 1d), the chemical shift observed between 7 and 8 ppm is ascribed to the hydrogen atoms situated within the benzene ring of PBA. Conversely, the peaks detected within the range of 1.5 to 2 ppm correspond to the hydrogen atoms associated with the carbonyl groups in the HA chain. A quantitative analysis of the ^{1}H-NMR signals determined the degree of substitution of phenylboronic acid (PBA) onto hyaluronic acid (HA) to be 58%. Meanwhile, the FTIR spectra of HA and HP also demonstrated the successful conjugation of PBA to the HA chain. The absence of the HA peak in HP at 1550 cm^{-1} is attributed to the C═O vibration of CONH.

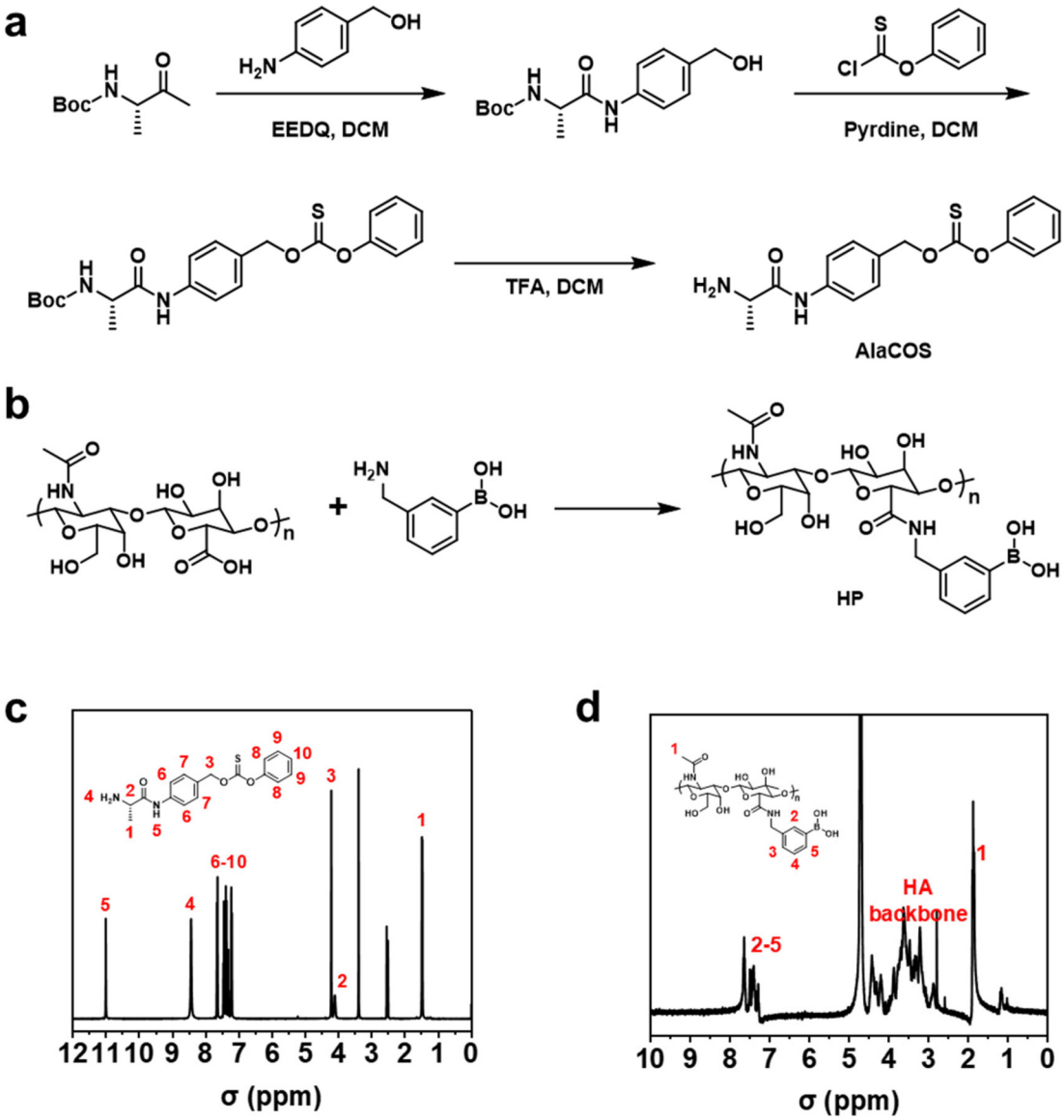

Fig. 1 Synthesis and characterization of AlaCOS and HP. The synthetic route of (a) AlaCOS and (b) HP. ^{1}H-NMR spectra of (c) AlaCOS and (d) HP.

3.2 Preparation and characterization of HP AC NPs

Then, the responsive HP-AC NPs were prepared, which can release H_2S in the presence of APN and CA. The HP-AC NPs were made by mixing HP and AlaCOS (Fig. 2a). TEM analysis revealed that the HP-AC NPs exhibited a spherical morphology with an average diameter of 152.3 ± 27.7 nm (Fig. 2b). Moreover, the HP-AC NPs exhibited a hydrodynamic diameter of 267.1 ± 7.1 nm and a negative charge (Fig. S3 and Fig. S4†). The efficient release of drugs is important to improve therapeutic outcomes. Given that the tissue fluid of psoriatic skin tends to be acidic, we investigated the release profiles of NPs at pH 5.5 and 7.4 (Fig. 2c) with reference to the calibration curve of AlaCOS in DIW (Fig. S5†). The results showed that AlaCOS could be released from HP-AC NPs under both neutral and acidic pH conditions. The release of AlaCOS at neutral pH

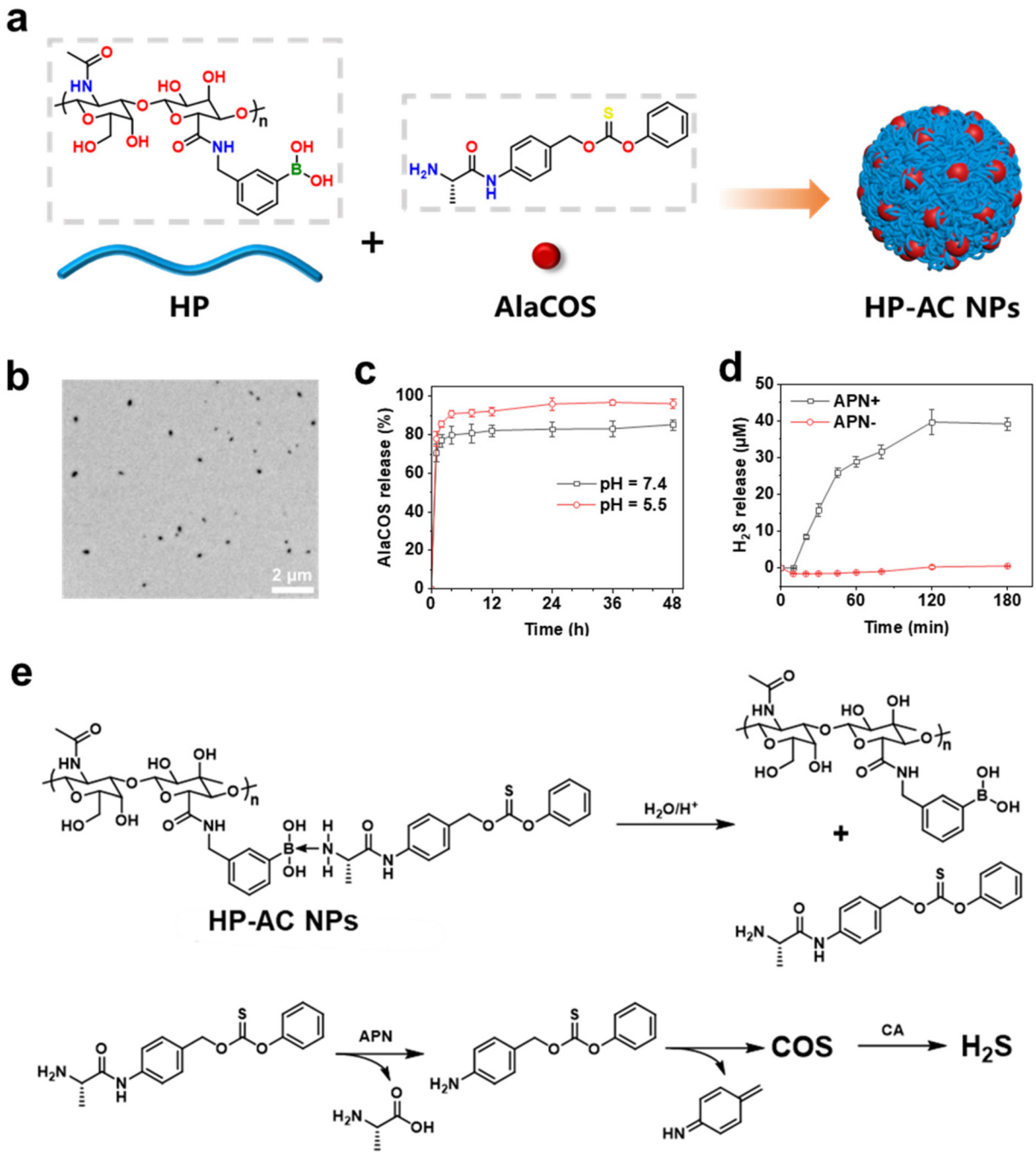

Fig. 2 Preparation and drug release of HP-AC NPs. (a) Schematic illustration of the preparation of HP-AC NPs. (b) TEM image of HP-AC NPs. (c) Release of AlaCOS from HP-AC NPs under different pH conditions (n = 3), and (d) the release of H_2S from HP-AC NPs with or without APN (n = 4). (e) The H_2S release mechanism from HP-AC NPs.

can be explained by the hydrolysis of boron–nitrogen coordination. In acidic conditions, the release of AlaCOS from HP-AC NPs reached 90.85% after 3 h, which was ~10% higher than the release observed at pH 7.4. Considering the acidic pH in psoriatic skin, the increased release rate in acidic pH is advantageous for achieving greater efficiency in treating psoriatic skin. Additionally, the assessment of the H_2S release capacity indicated that HP-AC NPs could effectively release H_2S in the presence of CA and APN. Without APN, no obvious H_2S release from HP-AC NPs was observed. Thus, the HP-AC NPs can achieve enzyme-responsive drug release (Fig. 2d).

Thus, the release mechanism of HP-AC NPs can be summarized as follows (Fig. 2e). Initially, the HP-AC NPs release AlaCOS upon contact with water or under acidic conditions. The amide bond in the released AlaCOS can be cleaved by APN, triggering a 1,6-elimination reaction that produces COS. This COS can be further catalyzed by CA to form H_2S.

3.3 The anti-inflammatory properties *in vitro*

We further demonstrate that HP-AC NPs exhibited anti-inflammatory functions *in vitro*. M1 macrophages play a significant role in the pathogenesis of psoriasis by producing various pro-inflammatory cytokines.[43,44] Therefore, inducing the transition from pro-inflammatory to anti-inflammatory macrophages could be a promising therapy for psoriasis.[45] Native RAW264.7 cells can be easily activated into a pro-inflammatory M1 phenotype when stimulated by lipopolysaccharides (LPS). Following incubation of M1 macrophages with Na_2S or HP-AC NPs (Fig. 3a), a comparative analysis of intracellular fluorescence signals revealed that the H_2S signal intensity in the HP-AC NPs-treated group was markedly higher than that observed in both the control and Na_2S-treated groups. This enhanced fluorescence indicates a superior intracellular H_2S release efficacy of HP-AC NPs. In addition, M1 phenotype macrophage was indicated by increased levels of nitric oxide (NO) and tumor necrosis factor-α (TNF-α) following LPS treatment (Fig. 3b and c). After LPS stimulation, the NO concentration increased by ~35.8%, while TNF-α expression nearly doubled compared to the control group. To evaluate the anti-inflammatory properties, the HP-AC NPs were compared with sodium sulfide (Na_2S) by examining their effects on NO concentration and TNF-α expression. The results indicated that both Na_2S and HP-AC NPs successfully induced anti-inflammatory macrophage polarization due to their H_2S release properties. The level of TNF-α in macrophages treated with HP-AC NPs was reduced compared to macrophages stimulated by LPS. Especially, incubating LPS-treated macrophages with HP-AC NPs reduced NO levels that approached those of the control group, which was significantly lower than the levels observed in the Na_2S group. The enhanced anti-inflammatory properties of HP-AC NPs are attributed to their controlled-release characteristics, in contrast to the rapid-release nature

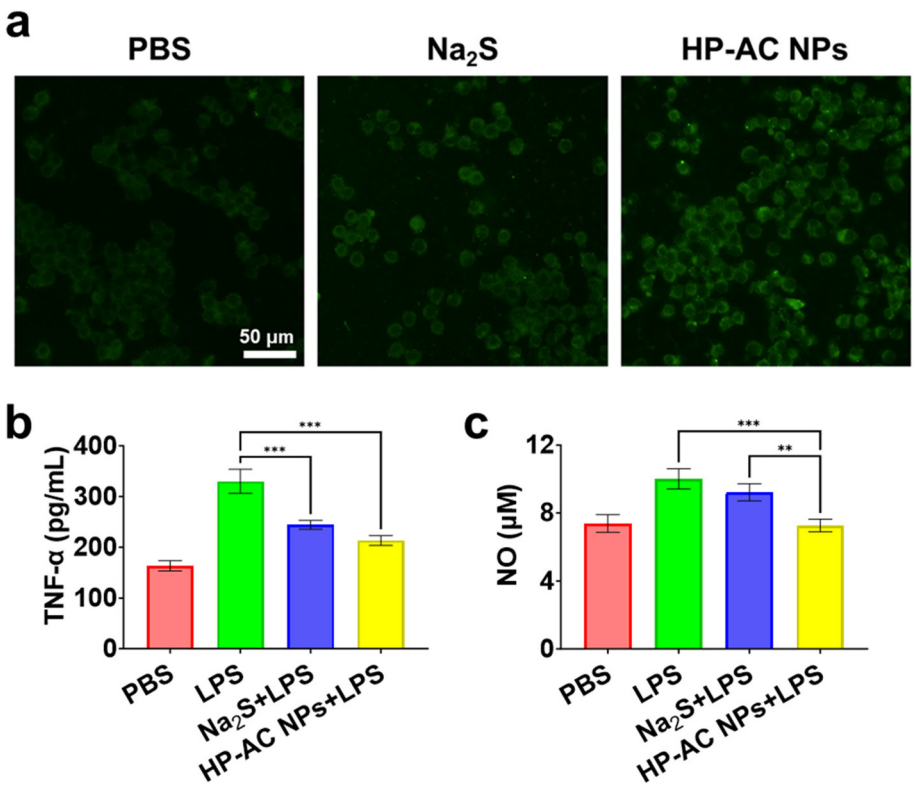

Fig. 3 The anti-inflammatory effect of HP-AC NPs *in vitro*. (a) Characterization of H_2S generation in RAW264.7 cells. (b) TNF-α content and (c) NO concentration in the culture medium of RAW264.7 cells treated with different materials. Data points represent mean ± s.d. (n = 3), ** P < 0.002, *** P < 0.001.

of Na_2S. In addition, we also performed flow cytometry to detect the expression of M2 macrophage marker CD206 (Fig. S6†). It was observed that the expression of CD206 in the HP-AC treatment group was increased by 95.43% compared with that in the Na_2S treatment group, which indicated a more effective psoriasis treatment.

3.4 Preparation and characterization of HP-AC MN

To enhance the therapeutic efficacy of HP-AC NPs, we loaded HP-AC NPs into MN patches (HP-AC MN), leveraging their superior delivery efficiency and minimally invasive transdermal application. A microfabrication method was used to fabricate HP-AC MN (Fig. S7†). Dermatoscopy and scanning electron microscope (SEM) were chosen to exam the morphology and architecture of the MN (Fig. 4a–c). The results indicated that the microneedle tips exhibited a regular square-based pyramid shape, with a height of 600 μm and a base diameter of 200 μm. To examine the penetration capacity of HP-AC MN, sodium fluorescein was selected as a label to be loaded into the MN (Fig. 4d). Fig. 4e illustrates that upon application to porcine skin, the MN achieved a penetration depth of up to 220 μm. Additionally, skin tissue was collected immediately after MN application for hematoxylin and eosin (HE) staining. The resulting holes in the skin from the MN puncture were observed, with a piercing depth of ~100 μm (Fig. S8†). Furthermore, the mechanical strength of the MN was assessed. The HP-AC MN had a fracture force of 0.5 N per needle, demonstrating their capacity to puncture the stratum corneum[46] (Fig. 4f). Additionally, the biocompatibility and non-invasiveness of MN were demonstrated by the rapid healing of the MN-treated mice skin within 1 h of post-application (Fig. 4g). These results highlight the MN as a safe and efficacious transdermal delivery system for the administration of HP-AC NPs into the skin to treat psoriasis. Additionally, the drug release from MNs was investigated. The release curve for AlaCOS in the HP-AC MNs was found to demonstrate results similar to those observed with HP-AC NPs. Under acidic conditions, it was noted that the drug release from the MNs reached 80.78% at 48 h, which was 13.11% higher compared to the release at pH 7.4 (Fig. S9†).

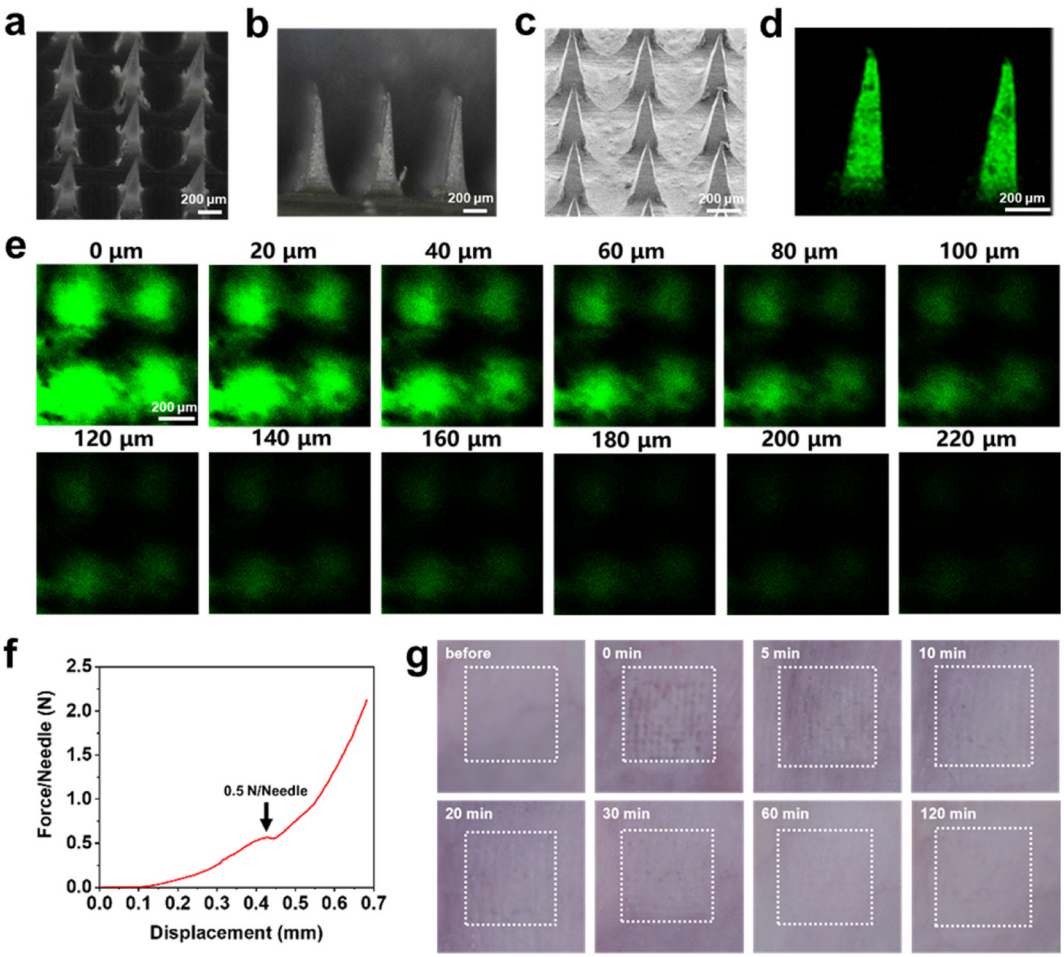

Fig. 4 Characterization of HP-AC MN. (a and b) Dermoscopic images of MN (c) SEM image of MN. (d) confocal laser scanning microscope (CLSM) image of MN labeled by fluorescein. (e) CLSM images of MN-treated skin exhibiting penetration depth of MN in the skin. (f) Mechanical strength test of MN. (g) Skin status at different time points after MN treatment.

3.5 Therapeutic effect of HP-AC MN on psoriasis mice

After the preparation of MN, we demonstrated that the HP-AC MN could alleviate psoriasis symptoms in a psoriasis mouse model. HP-AC MN was applied to the skin of imiquimod (IMQ)-induced psoriasis mice to evaluate the therapeutic efficacy. The mice were divided into four groups: control, model, 1 MN (1 MN applied at a time, 10 μg per MN), and 3 MN (3 MN applied at a time, 10 μg per MN). The psoriasis mouse model was established by applying IMQ cream to the mice over a six-day period. The administration of HP-AC MN occurred on days 3rd, 4th, and 5th to facilitate the treatment of psoriasis (Fig. 5a and Fig. S10†). The Psoriasis Area and Severity Index (PASI) score revealed that 3 MN exhibited a marked decrease in PASI scores compared to the model group (Fig. 5b). As shown in Fig. 5c and d, H&E. staining analysis of mouse skin indicated that the epidermal thickness in normal mice was 11.1 ± 1.9 μm. In contrast, the epidermal thickness in psoriasis-affected mice was significantly increased to 51.4 ± 7.5 μm due to IMQ treatment. Following treatment with either 1 or 3 HP-AC MN, the epidermal thickness decreased to 47.5 ± 5.9 μm and 38.3 ± 7.5 μm, respectively. These results confirm the therapeutic effectiveness of HP-AC NPs in treating psoriasis. The spleen index is an important indicator for evaluating the inflammatory status associated with psoriasis. As illustrated in Fig. 5e, the spleen index in the model group escalated to 14.6 ± 0.8, representing a 2.6-fold elevation compared to the control group. In contrast, the spleen index for the 1 MN and 3 MN treatment groups declined to 12.2 ± 1.9 and 10.4 ± 0.5, respectively, suggesting that a higher dosage of HP-AC NPs is more effective in mitigating the symptoms of psoriasis. In addition, we conducted a thorough safety assessment of the microneedle application. The mouse body weight, blood biochemical markers (ALT, AST, and UREA), and histological examinations of primary organs revealed that the administration of MN did not induce significant toxicological effects in mice (Fig. S11–S13†).

Finally, the therapeutic mechanism was invested through immunofluorescent analysis of proliferation and immune-related markers in the skin (Fig. 6 and Fig. S14†). The results indicated that the expression of cell proliferation-related protein, Ki-67, in the model group was upregulated compared

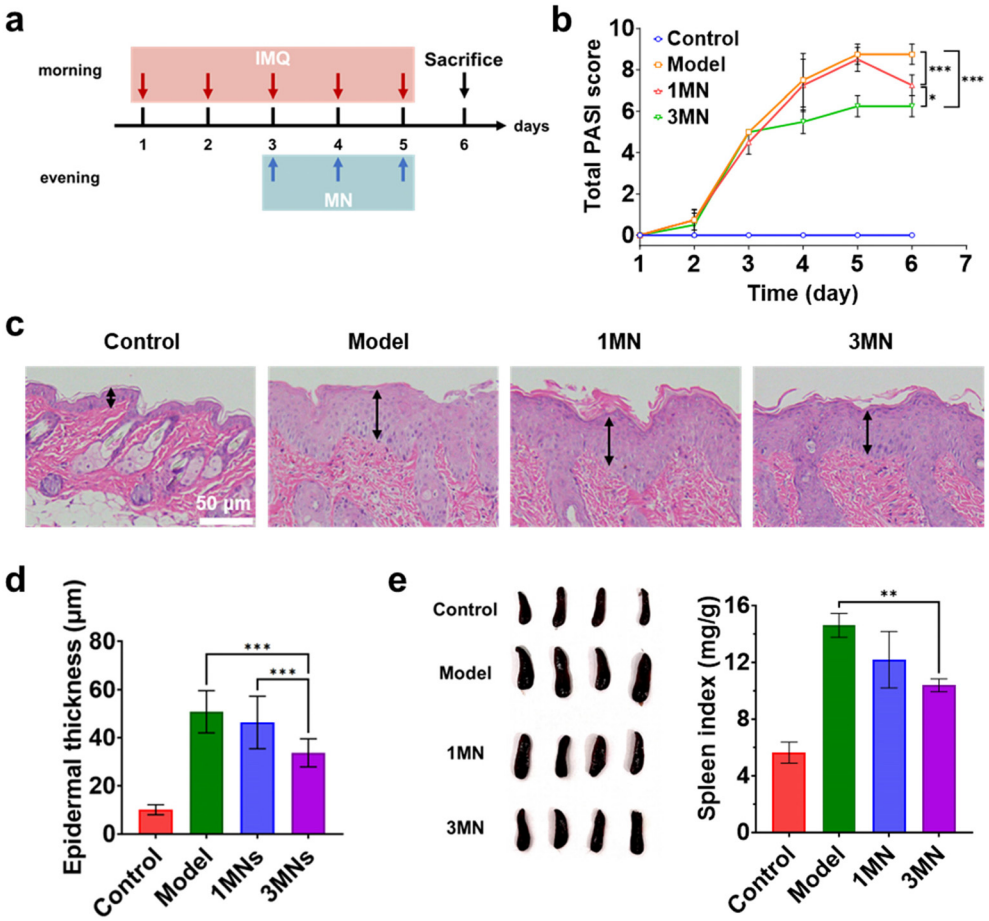

Fig. 5 *In vivo* evaluation of the therapeutic effect of HP-AC MN patch in a psoriasis mouse model. (a) Schematic illustration of the animal experimental schedule. (b) Total PASI scores of various groups. (c) Representative images of the H&E staining of skin tissue from various groups. (d) Skin thickness of the various groups. (e) Mice liver pictures and liver indexes of various groups. Data present as mean ± s.d. (n = 4 mice per group), * P < 0.033, ** P < 0.002, *** P < 0.001.

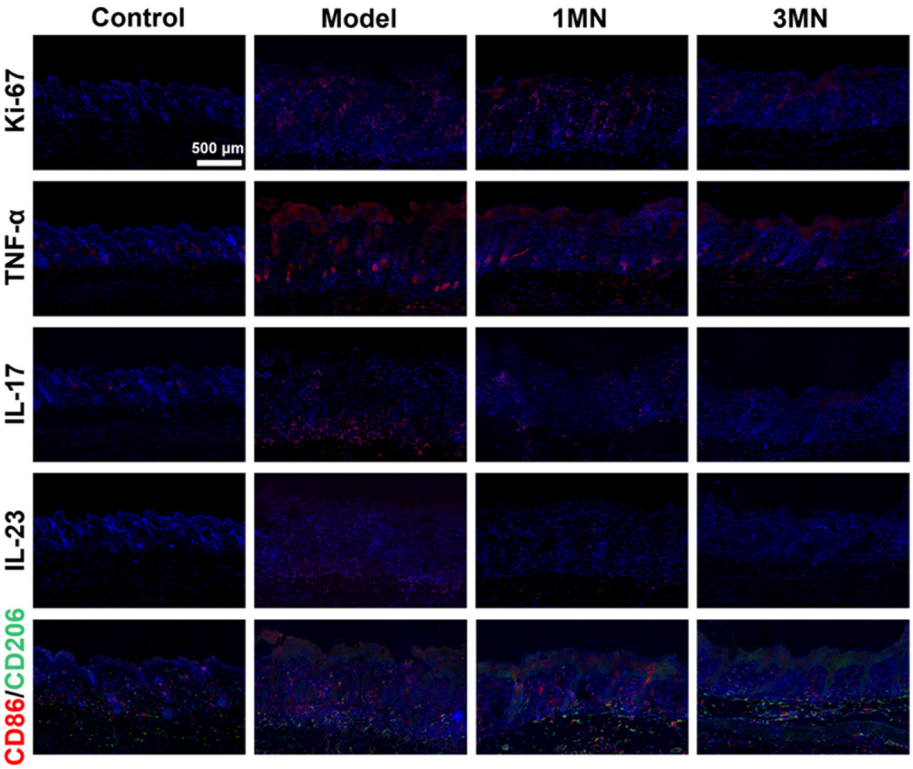

Fig. 6 Evaluation of cytokine expression and macrophage polarization in different treatment groups by immunofluorescent images. Cell proliferation markers (Ki-67), pro-inflammatory cytokines (TNF-α, IL-17, IL-23), and macrophage markers (CD86, CD206) are characterized in each group.

to the control group. The administration of HP-AC MN effectively diminished Ki-67 expression, with the 3 MN group exhibiting a significant decline, decreasing the expression relative to the model group. Moreover, the inflammatory cytokines in psoriatic skin, including TNF-α, IL-17, and IL-23, were analyzed. The results demonstrated that the 3 MN notably downregulated the expression of the relevant pro-inflammatory markers compared to the model group. Recognition of the critical role that macrophage polarization occupies in the inflammatory microenvironment associated with psoriasis, an assessment of M1 and M2 macrophage expression in the skin *via* immunofluorescence staining was performed. CD86 was utilized as a marker for M1 macrophages, while CD206 served as an indicator for M2 macrophages. As depicted in Fig. 6, the treatment group exhibited a marked increase in green fluorescence (CD206), alongside a decrease in red fluorescence (CD86), when compared to the model group. Thus, HP-AC MN effectively modulated the immune microenvironment in psoriatic lesions, reducing inflammation and inhibiting psoriasis progression.

4. Conclusions

In summary, we have demonstrated a responsive MN-mediated transdermal H_2S gas therapy for treating psoriasis. We synthesized the responsive H_2S donor and polymer carrier HP, which were assembled into HP-AC NPs. The obtained HP-AC NPs can efficiently release over 90% AlaCOS in an acidic environment. The released AlaCOS can undergo sequential catalysis by APN and CA, resulting in the liberation of H_2S. Compared to Na_2S, the HP-AC NPs exhibited enhanced H_2S generation ability in cells. The released H_2S from HP-AC NPs induced anti-inflammatory macrophage polarization, indicated by the reduction of NO and TNF-α levels compared to the LPS-treated macrophages. Furthermore, the HP-AC MNs were prepared with sufficient mechanical strength to penetrate the stratum corneum barrier. In the psoriatic mouse model, the mice receiving the HP-AC NP-loaded MN treatment exhibited decreased epidermal thickness, with higher doses of HP-AC NPs leading to better therapeutic outcomes. Immunofluorescence analysis showed that psoriatic skin treated with HP-AC MNs exhibited reduced expression of the proliferative marker Ki-67, along with decreased levels of inflammatory cytokines TNF-α, IL-17, and IL-23. Moreover, the HP-AC MN treatment induced the M2 polarization of macrophages. These results indicate the potential of HP-AC MN therapy to mitigate proliferation and inflammation in psoriasis. This MN-mediated H_2S gas therapy represents a promising alternative for treating psoriasis and may also apply to other inflammatory skin diseases.

Author contributions

Yanlin Wang: validation, data curation, visualization, investigation, formal analysis, and writing – original draft. Fan Rong:

validation, data curation, visualization, and investigation. Xiaoyi Sun: validation, data curation, visualization, and investigation. Duohang Bi: validation, data curation, visualization, and investigation. Yin Wang: conceptualization, supervision, and writing – review & editing; Yijing Liu: conceptualization, supervision, funding acquisition, writing – original draft, and writing – review & editing; Jintao Zhu: conceptualization, supervision, and writing – review & editing.

Data availability

The data supporting this article have been included as part of the ESI.†

Conflicts of interest

There are no conflicts to declare.

Acknowledgements

We gratefully acknowledge the National Natural Science Foundation of China (No. 52373138) and Shenzhen Science and Technology Program (GJHZ20240218114707015) for funding support. We also appreciate the Center for Experimental Chemistry (HUST) and Research Core Facilities for Life Science (HUST), which supplied the facility support.

References

1 J. M. Gelfand, *N. Engl. J. Med.*, 2024, **390**, 561–562.
2 J. Guo, H. Zhang, W. Lin, L. Lu, J. Su and X. Chen, *Signal Transduction Targeted Ther.*, 2023, **8**, 437–474.
3 G. Schett, P. Rahman, C. Ritchlin, I. B. McInnes, D. Elewaut and J. U. Scher, *Nat. Rev. Rheumatol.*, 2022, **18**, 311–325.
4 H. J. Lee and M. Kim, *Int. J. Mol. Sci.*, 2023, **24**, 12–23.
5 A. W. Armstrong and C. Read, *J. Am. Med. Assoc.*, 2020, **323**, 1945–1960.
6 M. L. Mourelle, C. P. Gómez and J. L. Legido, *Appl. Sci.*, 2024, **14**, 23–45.
7 C. Prandelli, C. Parola, L. Buizza, A. Delbarba, M. Marziano, V. Salvi, V. Zacchi, M. Memo, S. Sozzani, S. Calza, D. Uberti and D. Bosisio, *Int. J. Immunopathol. Pharmacol.*, 2013, **26**, 633–646.
8 R. Darlenski, I. Bogdanov, M. Kacheva, D. Zheleva, Z. Demerdjieva, E. Hristakieva, J. W. Fluhr and N. Tsankov, *J. Eur. Acad. Dermatol. Venereol.*, 2021, **35**, 196–198.
9 X. Fang, J. Wang, C. Ye, J. Lin, J. Ran, Z. Jia, J. Gong, Y. Zhang, J. Xiang, X. Lu, C. Xie and J. Liu, *Nat. Commun.*, 2024, **15**, 9071–9087.
10 F. Yang, W. Zhong, S. Pan, Y. Wang, Q. Xiao and X. Gao, *Biochem. Biophys. Res. Commun.*, 2024, **692**, 149343.
11 X. Shi, H. Li, F. Guo, D. Li and F. Xu, *J. Adv. Res.*, 2024, **58**, 105–115.
12 J. R. Rivers, A. Badiei and M. Bhatia, *Expert Opin. Ther. Targets*, 2012, **16**, 439–449.
13 M. Zhang, J. Cheng, Z. Shen, P. Lin, S. Ding and J. Hu, *Angew. Chem., Int. Ed.*, 2023, **62**, 202314563.
14 X. Dong, H. Zhang, P. Duan, K. Liu, Y. Yu, W. Wei, W. Wang, Y. Liu, Q. Cheng, X. Liang, Y. Huo, L. Yan, A. Yu and H. Dai, *Sci. Adv.*, 2023, **9**, 1078–1097.
15 Y. Zhu, W. R. Archer, K. F. Morales, M. D. Schulz, Y. Wang and J. B. Matson, *Angew. Chem., Int. Ed.*, 2023, **62**, 202302303.
16 A. Zhang, Q. Wei, Y. Zheng, M. Ma, T. Cao, Q. Zhan and P. Cao, *Adv. Healthcare Mater.*, 2024, **13**, 2400803.
17 F. Rong, T. J. Wang, Q. Zhou, H. W. Peng, J. T. Yang, Q. L. Fan and P. Li, *Bioact. Mater.*, 2023, **19**, 198–216.
18 C. R. Powell, K. M. Dillon and J. B. Matson, *Biochem. Pharmacol.*, 2018, **149**, 110–123.
19 A. K. Gilbert and M. D. Pluth, *J. Am. Chem. Soc.*, 2022, **144**, 17651–17660.
20 R. M. Mandel, P. S. Lotlikar, T. Runčevski, J.-H. Lee, J. J. Woods, T. A. Pitt, J. J. Wilson and P. J. Milner, *J. Am. Chem. Soc.*, 2024, **146**, 18927–18937.
21 F. Bellinato, P. Gisondi and G. Girolomoni, *Biol.: Targets Ther.*, 2021, **15**, 247–253.
22 A. Lloyd-Lavery, *Br. J. Dermatol.*, 2018, **179**, 815–816.
23 Y. Shi, J. Zhao, H. Li, M. Yu, W. Zhang, D. Qin, K. Qiu, X. Chen and M. Kong, *Adv. Healthcare Mater.*, 2022, **11**, 2200908.
24 B. H. J. Gowda, M. G. Ahmed, U. Hani, P. Kesharwani, S. Wahab and K. Paul, *Int. J. Pharm.*, 2023, **632**, 122591.
25 H. Wang, Y. X. Fu, P. Liu, F. Qu, S. Du, Y. Li, H. Y. Du, L. B. Zhang, J. Tao and J. T. Zhu, *ACS Appl. Mater. Interfaces*, 2023, **15**, 15162–15171.
26 W. Zhang, Y. Chen, Z. Zhao, H. Zheng, S. Wang, Z. Liao, T. Sheng, S. Zhao, W. Hou, X. Yu, F. He, J. Yu, Y. Zhang and Z. Gu, *Sci. Adv.*, 2023, **9**, 6007–6017.
27 L. Yang, D. Zhang, W. Li, H. Lin, C. Ding, Q. Liu, L. Wang, Z. Li, L. Mei, H. Chen, Y. Zhao and X. Zeng, *Nat. Commun.*, 2023, **14**, 7658.
28 F. Qu, Y. Sun, D. Bi, S. Peng, M. Li, H. Liu, L. Zhang, J. Tao, Y. Liu and J. Zhu, *Adv. Healthcare Mater.*, 2023, **12**, 2302314.
29 Y. Chen, J. Zhu, J. Ding and W. Zhou, *Chin. Chem. Lett.*, 2024, **35**, 108706.
30 W. Yang, X. Guo, R. Wu, Y. Wu, M. Fan, B. Lv, D. Zhang and Z. Zhu, *Energy Storage Mater.*, 2024, **5**, 99–107.
31 Y. Yi, Z. Yang, C. Zhou, Y. Yang, Y. Wu and Q. Zhang, *Nano TransMed*, 2024, **3**, 100030.
32 Y. Liu, X. Dai, B. Yu, M. Chen, N. Zhao and F.-J. Xu, *Biomater. Sci.*, 2022, **10**, 2618–2627.
33 N. Zhao, Z. Jiao, L. Chen, Z. Liu, X. Zhao and F.-J. Xu, *Acc. Mater. Res.*, 2023, **4**, 1068–1082.
34 Y. Zheng, S. H. Ley and F. B. Hu, *Nat. Rev. Endocrinol.*, 2018, **14**, 88–98.

35 F. Rong, W. Bao, G. Li, Y. Ge, W. Zhu, B. Hao, Y. Zhao, Y. Yuan and Y. Wang, *Angew. Chem., Int. Ed.*, 2025, **64**(14), e202423527.
36 C. Lu, M. A. Amin and D. A. Fox, *J. Immunol.*, 2020, **204**, 3–11.
37 H. Barker, M. Aaltonen, P. Pan, M. Vähätupa, P. Kaipiainen, U. May, S. Prince, H. Uusitalo-Järvinen, A. Waheed, S. Pastoreková, W. S. Sly, S. Parkkila and T. A. H. Järvinen, *Exp. Mol. Med.*, 2017, **49**, e334.
38 D. Antal, S. Alimohammadi, P. Bai, A. G. Szöllősi and M. Szántó, *Life*, 2022, **12**, 234.
39 W. Jungkunz, M. Eichhorn, J. Wörl, W. C. Marsch and H. Holzmann, *Arch. Dermatol. Res.*, 1992, **284**, 146–149.
40 W. Xiao, R. Geng, D. Bi, Y. Luo, Z. Zhang, Q. Gan, Y. Liu and J. Zhu, *Small*, 2024, **20**, 2308790.
41 R. Wang, X. Xu, D. Li, W. Zhang, X. Shi, H. Xu, J. Hong, S. Yao, J. Liu, Z. Wei, Y. Piao, Z. Zhou, Y. Shen and J. Tang, *Biomaterials*, 2022, **288**, 121737.
42 S. Lv, Y. Wu, K. Cai, H. He, Y. Li, M. Lan, X. Chen, J. Cheng and L. Yin, *J. Am. Chem. Soc.*, 2018, **140**, 1235–1238.
43 D. Kuraitis, N. Rosenthal, E. Boh and E. McBurney, *Arch. Dermatol. Res.*, 2022, **314**, 133–140.
44 S. H. Lin, H. Y. Chuang, J. C. Ho, C. H. Lee and C. C. Hsiao, *Arch. Dermatol. Res.*, 2018, **91**, 276–284.
45 L. Li, H. Zhang, X. Zhong, Y. Lu, J. Wei, L. Li, H. Chen, C. Lu and L. Han, *Life Sci.*, 2020, **243**, 117231.
46 M. Sang, M. Cho, S. Lim, I. S. Min, Y. Han, C. Lee, J. Shin, K. Yoon, W. H. Yeo, T. Lee, S. M. Won, Y. Jung, Y. J. Heo and K. J. Yu, *Sci. Adv.*, 2023, **9**, 1765.